HAUBOLD, H. G. (1975). *J. Appl. Cryst.* **8**, 175–183.

IIJIMA, S. (1976). *34th Ann. Proc. Electron Microsc. Soc. Am.* Edited by G. W. BAILEY, pp. 490–491. Baton Rouge, Louisiana: Claitors Publ. Div.

IIJIMA, S. (1977). *Optik.* **43**, 193–214.

KRAKOW, W., CHANG, A. L. J. & SASS, S. L. (1977). *Philos. Mag.* In the press.

KUWABARA, S. & UEFUJI, T. (1975). *J. Electron Microsc.* **24**, 137–144.

SKARNULIS, A. J. (1975). PhD Thesis, Arizona State Univ.

SKARNULIS, A. J., IIJIMA, S. & COWLEY, J. M. (1976). *Acta Cryst.* A **32**, 799–805.

SPENCE, J. C. H. (1975). *Developments in Electron Microscopy and Analysis*, Edited by J. A. VENABLES, p. 257. New York: Academic Press.

SPENCE, J. C. H. (1977). In *35th Ann. Proc. Electron Microsc. Soc. Am.* Edited by G. W. BAILEY, pp. 178–179. Baton Rouge, Louisiana: Claitors Publ. Div.

Approximations for Dynamical Calculations of Microdiffraction Patterns and Images of Defects

BY JOHN C. H. SPENCE

Arizona State University, Department of Physics, Tempe, Arizona 85281, USA

The calculation of dynamical elastic diffuse electron scattering from a crystal containing a point defect or dislocation may require prohibitively large amounts of computing time. Two approximations are described which greatly reduce the computer time required for these calculations, and so allow the simulation of electron-microscope images of defects at atomic resolution. The diffuse scattering expected from microdiffraction experiments can also be predicted in this way.

1. Introduction

Recent instrumental developments in high-resolution transmission electron microscopy have led to the production of a generation of instruments capable of producing high-quality images showing a point resolution of perhaps 3·5 Å and, in favorable cases, lattice resolution better than 1·0 Å. Image detail from metallurgical specimens on this scale cannot be interpreted with the conventional theory of diffraction contrast from imperfect crystals based on the column approximation (see, for example, Hirsch, Howie, Nicholson, Pashley & Whelan, 1965). The most recent development of this theory, the weak-beam method, allows an interpretation of detail on electron micrographs down to perhaps 15 Å. Despite the considerable success of diffraction contrast theory for the characterization of dislocations and the investigation of their interactions, much recent interest has centered on the development of theoretical methods to allow the fullest use of present-day instrumental capabilities. Rather than obtaining contrast from the defect strain field in a single-beam image as in conventional metallurgical microscopy, the aim is to use the methods of lattice imaging (Menter, 1956; Cockayne, Parsons & Hoelke, 1971; Iijima, 1975) and single-atom imaging (Hashimoto, Kumao, Hino, Yotsumoto & Ono, 1973) to expose the structure of the defect at high resolution. There is some hope that by matching computer-simulated trial structure images and diffraction patterns with experimental recordings, the detailed atomic structure of a defect may be revealed. The necessary experimental images and diffraction patterns can now be recorded under closely specified experimental conditions with, for the image, known values of defocus, spherical and chromatic aberration constants, incident-beam divergence and specimen orientation (see, for example, Krivanek, 1976).

Experience in our laboratory has shown that the computer simulation of these high-resolution electron images requires very large amounts of computer time. For example, a recent 500-beam dynamical calculation showing through-focus images from an interstitial defect in a lead film (thickness 80 Å) required 10 min computing time on a Univac 1110-42 computer. This raises serious questions about the usefulness of image simulation as a tool for the structure analysis of defects.

The purpose of this note is to outline two approximations which can be made to reduce the amount of computing time required by use of the multislice method. Methods for calculating the coherent scattering from non-periodic specimens have been known for some time in X-ray diffraction (see, for example, Krivoglaz & Ryaboshapka, 1963); however, calculations for electron scattering where dynamical scattering may be important are a more recent development (Grinton & Cowley, 1971; Cockayne, 1976).

2. Diffuse scattering under plane-wave illumination

By use of the method of periodic continuation, a large superlattice containing the defect is constructed and the scattering calculation performed in the usual way with the superlattice treated as a single unit cell. This method of calculation, which gives the elastic diffuse scattering between Bragg reflections, should be clearly distinguished from the so-called 'non-column approximation' calculations which yield values of the scattered amplitude only in the directions of Bragg reflections. In order to avoid artifacts it is important that the implied periodic extension of this cell potential is smoothly connected at the cell edges (Lanczos, 1966). In addition, it must be borne in mind that these computed images are the images which would be obtained from a periodic array of defects and so may differ under certain experimental conditions (of focus, for example) from the image of an isolated defect. By making the superlattice cell sufficiently large, it is possible to make these differences negligible. For a one-dimensional superlattice of length $X = n_a a_0$ (a_0 is the periodicity of the perfect crystal), the calculation produces sampled values of the elastic diffuse scattering at intervals $u = 1/X = \Delta\theta/\lambda$ with θ the scattering angle. Bragg reflections occur at $\theta/\lambda = n_a/X = 1/a_0$. Calculations based on the multislice method allow the structure to be varied as a function of depth through the crystal. The N-beam iterative equation used is then

$$\psi^{n+1}(\mathbf{h}) = \sum_{\mathbf{g}} \psi^n(\mathbf{g}) P(\mathbf{g}) Q_n(\mathbf{h} - \mathbf{g}) \qquad (1)$$

with $\psi^n(\mathbf{g})$ proportional to the amplitude of the Bragg reflection g emerging from the nth slice. More details of this equation can be found in Goodman & Moodie (1974) and Cowley (1975). Here $P(\mathbf{g})$ is the propagator

$$P(\mathbf{g}) = \exp(-2\pi i S_\mathbf{g} \Delta z)$$

with Δz the slice thickness and $S_\mathbf{g}$ the excitation error for beam $\mathbf{g}$ ($S_\mathbf{g}$ is positive for a reflection inside the sphere). Here $Q_n(\mathbf{h}) \Delta z$ is proportional to the amount of new scattering generated in the slice in direction $\mathbf{h}$. The scattering amplitudes $Q_n(\mathbf{h})$ have conventionally been taken to be the Fourier coefficients of

$$\varphi^n(\mathbf{r}) = \exp[-i\sigma\varphi_p^n(\mathbf{r})] \qquad (2)$$

where $\sigma = \pi/\lambda V_0$ (non-relativistic) and $\varphi_p^n(\mathbf{r})$ is a projection through the slice potential taken in the direction of the crystal zone axis nearest the incident-beam direction. Here $\mathbf{r}$, $\mathbf{g}$ and $\mathbf{h}$ are two-dimensional vectors in the plane to which this zone axis is normal. Equation (2) takes account of multiple scattering within the slice. Its first-order expansion,

$$\varphi^{n'}(\mathbf{r}) = 1 - i\sigma\varphi_p^n(\mathbf{r}) \qquad (3)$$

with Fourier coefficients

$$\bar{Q}_n(\mathbf{h}) = -i\sigma V^n(\mathbf{h}) \Delta z \qquad \text{for } \mathbf{h} \neq 0$$

$$= 1 - i\sigma V^n(0) \Delta z \quad \text{for } \mathbf{h} = 0, \qquad (4)$$

gives the kinematic scattering amplitudes. Here $V^n(\mathbf{h})$ is a Fourier coefficient of the crystal potential for the nth slice. For sufficiently thin slices (small Δz), the use of $\bar{Q}_n(\mathbf{h})$ in (1) in place of $Q_n(\mathbf{h})$ gives accurate results as pointed out by Lynch (1974), who described an efficient method of computing higher-order approximations for $Q_n(\mathbf{h})$. The use of kinematic amplitudes $\bar{Q}_n(\mathbf{h})$ has been investigated and found to give accurate results for light elements with Δz taken equal to the thickness of a layer of atoms. The resulting time saving is greatest for specimens for which the atomic structure is not periodic in the beam direction, such as an interstitial defect or dislocation in certain orientations. The use of $Q_n(\mathbf{h})$ would then require two digital fast Fourier transforms at each slice in addition to the structure-factor calculation for each slice. For silicon, the *Pendellösung* curves from a 25-beam calculation using the $\bar{Q}_n(\mathbf{h})$ have been compared with the results of a conventional calculation [equation (1)]. At 100 kV incident electron energy, and with a slice thickness of 2·33 Å, the various dynamical extinction distances were found to agree to within less than 3% for a wide range of excitation errors. A disadvantage of the use of kinematic scattering amplitudes is that, unlike the conventional multislice calculations, a unity sum of beam intensities does not indicate the inclusion of all reflections of appreciable intensity. However, for many light-element defect structures of technological importance this approximation makes possible the simulation of two-dimensional electron images which would be unrealistically time-consuming otherwise.

A second useful approximation in dynamical defect-image calculations is based on the neglect of double-diffuse scattering terms. Since these form by far the largest single group of terms in (1) for imperfect specimens, a considerable saving in computing time is possible. The bulk of the computing time used for a structure periodic in the beam direction is taken up in the evaluation of the convolution sums in (1). Writing (1) in one dimension with an artificial superlattice again of length $X = n_a a_0$, we can distinguish four partial sums:

$$\psi^{n+1}(h) = \sum_{\substack{g \neq mn_a \\ (h-g) \neq mn_a}} \psi^n(g) P(g) Q(h - g)$$

$$+ \sum_{\substack{g \neq mn_a \\ (h-g) = mn_a}} \psi^n(g) P(g) Q(h - g)$$

$$+ \sum_{\substack{g = mn_a \\ (h-g) \neq mn_a}} \psi^n(g) P(g) Q(h - g)$$

$$+ \sum_{\substack{g = mn_a \\ (h-g) = mn_a}} \psi^n(g) P(g) Q(h - g)$$

$$(m = 0, \pm 1, \pm 2 \ldots). \qquad (7)$$

Here the indices g and h refer to the sampled values of the elastic diffuse scattering along the systematics line.

Every n_ath such 'beam' is a Bragg reflection. The physical interpretation of these four terms is as follows. The first describes the scattering of diffuse scattering incident on the nth slice into a new diffuse (non-Bragg) direction. The second describes the scattering of incident diffuse scattering into a new Bragg direction, while the third describes the scattering of incident Bragg beams into diffuse (non-Bragg) directions. The final partial sum is zero if the wanted beam h is not a Bragg reflection ($h \neq mn_a$) while the second and third terms are zero where h denotes a Bragg reflection. Since the number of diffuse 'beams' far exceeds the number of Bragg reflections in all practical cases, the partial sum with the largest number of terms in any calculation is the first. This is also the smallest, since it represents the sum of products of small numbers. The effect of neglecting this term is indicated in Fig. 1 for a particular defect. This shows the elastic diffuse scattering expected along the [022] systematics line in an aluminium foil due to an undissociated edge dislocation with Burgers vector $\frac{1}{2}[110]$. The foil normal and incident-beam direction is $[\bar{1}11]$ and the crystal potential has been projected in the $[1\bar{1}2]$ direction. The dislocation core structure is obtained by the method of Cotterill & Doyama (1966) (their 'elasto-atomic' model) and is not expected to be accurate; however, small displacements of core atoms have little effect on the diffuse intensity distribution (but a large effect on the high-resolution image). Two-dimensional calculations based on more sophisticated core-structure

models are in preparation. The neglect of diffuse–diffuse scattering terms is seen to have negligible effect on the calculated intensities. The line broadening seen is similar to that observed in X-ray diffraction, which, in the kinematic approximation, is proportional to the variance of the strain-field distribution function.

The saving in computing time resulting from the neglect of these terms can be estimated as follows. The total number of terms in (1) for N beams (including diffuse 'beams') and all possible values of h is

$$S_N = (3N^2 + 1)/4 \quad (N \text{ odd}),$$

while the number of terms in the second, third and fourth partial sum of (7) (for all h) is

$$S_{BQ} = n_B + \frac{3n_B^2 - 4n_B + 1}{4} (2n_a - 1),$$

where n_B is the number of Bragg reflections. Here $N = (n_B - 1)n_a + 1$. The fractional reduction in computing time if only these terms are included is $1 - F$ where

$$F = S_{BQ}/S_N.$$

For a typical calculation, $n_B = 17$, $n_a = 40$ and $N = 641$ giving $F = 0\cdot05$. Thus, the time taken to perform the convolution of (1) is reduced by 95% if diffuse–diffuse scattering terms are excluded from the calculation. In practice this is easily done using modulo arithmetic. By use of the relation between the multislice, Darwin and Matrix theories (Johnson, 1968) an equivalent approximation can be developed for these theories.

The effect of the neglect of these terms on image synthesis has also been investigated. Images formed in bright field from the elastic diffuse scattering were barely affected by the neglect of the double-diffuse scattering terms, the variation in image intensity being less than 1% for a wide range of orientations and simulated experimental conditions. Under conditions of limited resolution, these images resemble the conventional metallurgical diffraction-contrast images.
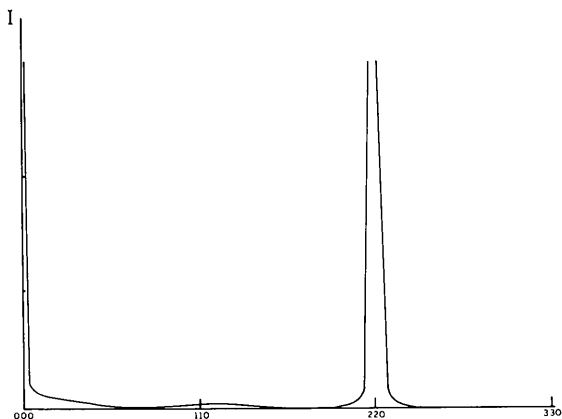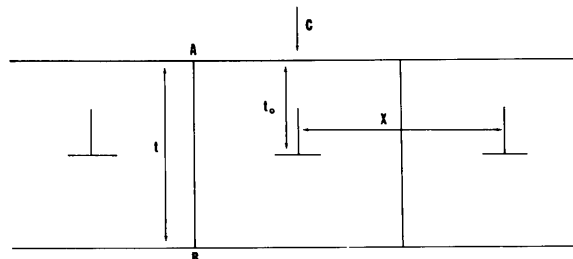

Fig. 1. Computed elastic diffuse scattering along the [220] systematics line due to the array of dislocations shown in Fig. 2. On the scale of this diagram it is not possible to distinguish the result of the calculation which includes diffuse–diffuse terms from that which omits these terms. The height of the Bragg peaks (not shown) depends on the area of specimen illuminated. With an illuminated area of 80 Å² the angular half width of the 220 reflection is 1·5 mrad at 100 kV. In this symmetrical zone-axis orientation (incident electron beam coincident with the [111] crystal direction) the diffuse scattering is symmetrical about the origin.

Fig. 2. The periodic array of dislocations used in calculations. The crystal thickness $t = 85$ Å, the dislocation depth $t_0 = 35$ Å and the distance between dislocations $x = 85$ Å. The incident-beam direction is indicated at C. A line of zero strain exists at the superlattice boundary along AB.

An important problem in defect-image simulation concerns the range of the defect strain field. For a displacement field which decays inversely with distance from the defect a discontinuity in the slope of the crystal potential is introduced at the artificial superlattice boundary whose magnitude may be a function of depth in the crystal. While this has only a small effect on simulated images of the defect at limited resolution, it may have a large effect on the calculated diffuse scattering. As shown in Fig. 2, this problem has been overcome in the present calculations by the application of periodic boundary conditions to the strain field. Thus, the calculations show the images and diffuse scattering which would result from a periodic array of dislocations.

Since the strains from adjacent dislocations exactly cancel along AB, this procedure produces a super-lattice whose size is independent of depth in the crystal.

3. Microdiffraction

For calculations of microdiffraction patterns in scanning transmission electron microscopy (STEM) under 'critical' illumination it is necessary to consider the form of the wavefield incident on the specimen. At one extreme of approximation this may be taken equal to the normalized complex impulse response of the probe-forming (objective) lens. The first slice in (1) then contains the Fourier coefficients $\psi^0(g)$ of this function, proportional to

$$\psi_0(g) = H(g)\exp[(i\pi/2)(C_s\lambda^3g^4 + 2\Delta f\lambda g^2)] \quad (8)$$

for an objective lens at defocus Δf with spherical aberration constant C_s. Here Δf is taken positive if a plane conjugate to the electron source falls on the source side of the specimen. $H(g)$ is a pupil function describing the
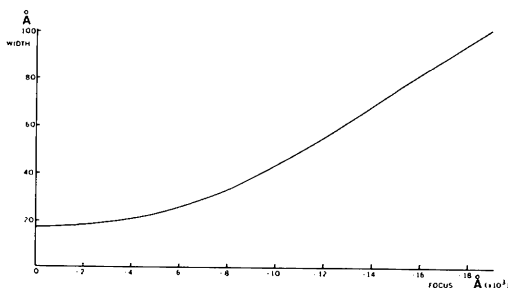

Fig. 3. Width of a coherent scanning-microscope probe as a function of focus setting. The negative focus defect refers to a lens weakened from the Gaussian focus condition where the source and specimen planes are conjugate. An electron source of negligible dimensions is assumed. For $C_s < 2$ mm and an objective aperture semiangle $\theta_{ap} = 0.002$ rad the probe size is controlled by the focus defect Δf alone if $|\Delta f| > 5000$ Å and is symmetrical with respect to Δf. For $|\Delta f| < 5000$ Å the curve is drawn for $\theta_{ap} = 0.002$ rad and $C_s = 1.5$ mm. The energy spread of the electron beam has been neglected. Accelerating voltage 100 kV.

objective lens aperture. Equation (8) is a good approximation if the lateral coherence width X_c in the exit pupil of the objective lens exceeds the diameter d of the exit pupil. This is commonly taken to be the objective aperture, so that we require very approximately

$$d < X_c \quad \text{where } X_c = \frac{\lambda}{2\pi\theta_s} \quad (9)$$

for a coherent probe at the specimen. Here θ_s is the semiangle subtended by the focused scan spot (strictly the geometrical source image) at the objective lens aperture. This angle depends both on the demagnification of the probe-forming lens and on the electron-source size. Equation (9) is satisfied under some STEM operating conditions; if it is not, partially coherent calculations must be carried out in which diffracted intensities are summed for each point on the electron source. An experimental method for determining the degree of coherence across an illuminating aperture has been described by Dowell & Goodman (1973).

In order to use the method of periodic continuation to approximate diffraction by a single (non-periodic) electron source it is important that the incident wavefunction at the specimen falls to negligible amplitude at the superlattice boundary. The width of the probe is a function of Δf, C_s and the objective aperture size for a diffraction-limited or aberration-limited probe. At large defocus or small aperture size these parameters may then be more important than the range of the defect strain field in determining the size of the artificial superlattice needed in calculations. Fig. 3 shows the width of the impulse response of an electron lens with $C_s = 1.5$ mm as a function of defocus. For most of the curve the impulse response is aberration limited and independent of the aperture size used if this is greater than 2 mrad. The width is taken as the distance between points on the specimen for which the probe intensity has fallen to 5% of its maximum value and gives an approximate indication of the size of artificial superlattice needed to simulate microdiffraction patterns under specified conditions of focus, spherical aberration and objective aperture size. The physical mechanism of diffraction by a coherent diffraction-limited focused probe has been discussed by Cowley & Jap (1976). Detailed calculations have also been made based on the method described above, which show the two-dimensional intensity distribution in the coherent convergent-beam microdiffraction pattern from the core of an edge dislocation in iron (Spence, 1977).

4. Conclusions

The development of quantitative methods for structure analysis by electron diffraction and imaging depends on our ability to compute the expected images and diffraction patterns from trial structures. With conventional computing methods an inordinate amount of

computing time is required for these calculations for non-periodic specimens if dynamical scattering and all electron optical parameters are included. The approximations outlined above make possible the simulation of these images and diffraction patterns within reasonable computing times. They therefore allow the possibility of least-squares refinement between computed images of trial structures and experimental many-beam images of defects.

References

COCKAYNE, D. J. H. (1976). *Proc. 6th Eur. Conf. Electron Microsc.*, Jerusalem, Israel, Vol. I. pp. 109–113.

COCKAYNE, D. J. H., PARSONS, J. R. & HOELKE, C. W. (1971). *Philos. Mag.* **24**, 139–153.

COTTERILL, R. M. J. & DOYAMA, M. (1966). *Phys. Rev.* **145**, 465–478.

COWLEY, J. M. (1975). *Diffraction Physics.* Amsterdam: North-Holland.

COWLEY, J. M. & JAP, B. K. (1976). *Tutorials on Scanning Electron Microscopy*, Chicago, Vol. I, pp. 378–384. Chicago: IIT Research Institute.

DOWELL, W. C. T. & GOODMAN, P. (1973). *Philos. Mag.* **28**, 471–473.

GOODMAN, P. & MOODIE, A. F. (1974). *Acta Cryst.* A**30**, 280–290.

GRINTON, G. & COWLEY, J. M. (1971). *Optik*, **34**, 221–233.

HASHIMOTO, H., KUMAO, A., HINO, K., YOTSUMOTO, H. & ONO, A. (1973). *Jpn. J. Appl. Phys.* **10**, 1115–1122.

HIRSCH, P. B., HOWIE, A., NICHOLSON, R. B., PASHLEY, D. W. & WHELAN, M. J. (1965). *Electron Microscopy of Thin Crystals.* London: Butterworths.

IIJIMA, S. (1975). *Acta Cryst.* A**31**, 784–790.

JOHNSON, A. W. S. (1968). *Acta Cryst.* A**24**, 534–543.

KRIVANEK, O. L. (1976). *Optik*, **45**, 97–100.

KRIVOGLAZ, M. A. & RYABOSHAPKA, K. P. (1963). *Fiz. Met. Metalloved.* **15**, 18–28.

LANCZOS, C. (1966). *Discourse on Fourier Series.* London: Oliver and Boyd.

LYNCH, D. (1974). *Acta Cryst.* A**30**, 101–102.

MENTER, J. W. (1956). *Proc. R. Soc. London, Ser. A*, **236**, 119–126.

SPENCE, J. C. H. (1977). *Proc. 35th Ann. EMSA Meet.* Boston, USA, pp. 178–179.

Use of Lattice Imaging in the Electron Microscope in the Structure Determination of the 126*R* Polytype of SiC

BY MADAN DUBEY AND G. SINGH

Department of Physics, Banaras Hindu University, Varanasi-221005, India

Lattice fringes corresponding to (00.3) spacings of the 126*R* polytype of SiC have been obtained in the electron microscope. A number of 10.*l* reflections were allowed to pass through the objective aperture to obtain the lattice fringes showing a periodicity of ~105 Å (one third of the *c* parameter of the hexagonal cell) and each unit-cell block is subdivided into smaller blocks corresponding to the spacings of 6*H*, 15*R*, 21*R* etc. The stacking sequence of these blocks has been used to work out the detailed structure of the 126*R* polytype. It has been suggested that the lattice resolution technique in conjunction with X-ray diffraction is likely to prove a useful method for determining difficult polytypic structures.

Introduction

There are a number of substances like SiC, ZnS, CdI_2 etc. which are known to crystallize in many unique periodicities and crystal structures. SiC polytypes are characterized by the number of Si–C double layers and their stacking sequence in the unit cell. Out of the various polytypes, 6*H* is the most commonly occurring structure followed by 15*R* and 4*H* in order of frequency of occurrence. A unique feature of the high-period polytypes of SiC is that their unit cells are built

up by stackings of the unit cells of more common structures of SiC like 6*H*, 15*R*, 4*H* etc. For example the structure of the 39*H* polytype of SiC expressed in Zhdanov notation is $(33)_2\ 32(33)_2\ (32)_2$ which clearly shows that its unit cell consists of four unit cells of 6*H* and three unit cells of 15*R* stacked in a sequence represented by the sequence of 33 and 32 in this symbol (Azuma, Ohta & Tomita, 1963).

When a high-period unit cell is dominantly built up of units of one small-period structure, its structure determination becomes comparatively simple. However